Effect of DNA Scaffolding on Intramolecular Electron Transfer Quenching of a Photoexcited Ruthenium(II) Polypyridine Naphthalene Diimide

Dabney W. Dixon,*,† Nancy B. Thornton, Vera Steullet, and Thomas Netzel*

Department of Chemistry, Georgia State University, Atlanta, Georgia 30303

Received November 8, 1997

Intramolecular emission quenching of a photoexcited ruthenium(II) polypyridine by a covalently linked naphthalene diimide (NDI) has been measured in aqueous buffer both without and with calf thymus DNA. The complex consists of a Ru(2,2′-bipyridine)$_2$(2,2′-bipyridine-5-carboxamide)$^{2+}$ electron donor covalently attached by way of a $-CH_2CH_2CH_2-$ linker to a 1,4,5,8-naphthalene diimide acceptor (Ru−NDI, **1**). The NDI portion of the complex intercalates in calf thymus DNA, as indicated by the hypochromism of its optical absorbance bands and observation of an induced circular dichroism spectrum in the same region. Emission quenching in Ru−NDI has been measured relative to a Ru tris-bpy model lacking the NDI moiety by both lifetime and emission quantum yield techniques. Using lifetime averages, the relative emission quenching is, respectively, 99.1% and 97.9% in aqueous buffer solutions without and with DNA. The emission quenching is ascribed to intramolecular electron transfer within the Ru−NDI complex with an estimated driving force ($-\Delta G°$) of 0.33 eV. In buffer, the emission decays of Ru−NDI alone are fit well with a triexponential model with lifetimes of 0.34 (0.88), 1.99 (0.11), and 12.6 (0.008) ns (relative amplitude). The emission decays of the DNA-intercalated Ru−NDI complex are also fit well with a triexponential model with lifetimes of 0.31 (0.79), 2.00 (0.13), and 11.8 (0.08) ns. Thus, the fractional amplitudes of the lifetimes change upon DNA intercalation of the complex, while the lifetimes themselves remain essentially the same. The average rates of electron transfer in aqueous buffer without and with DNA are, respectively, 1.6×10^9 and 6.8×10^8 s^{-1}. The striking result of this study is that the overall character of electron transfer quenching in Ru−NDI is very similar whether or not it is bound to DNA. Intercalation of the NDI in DNA apparently has negligible consequences for electron transfer, implying either that the activation energy and electronic coupling in Ru−NDI are largely unaffected by this, at first glance, seemingly significant environmental change or that changes in these parameters on DNA binding cancel fortuitously.

Introduction

Intramolecular electron transfer within covalently attached donor−linker−acceptor complexes has been the focus of intensive study in recent years.[1−14] These model systems facilitate the study of electron transfer reactions because they allow, in principle, the direct measurement of the forward and reverse electron transfer rates. In general, rigid linkers have been employed to hold the donor and acceptor moieties at well-defined distances and orientations. Some studies, however, have probed the effect of scaffolding on controlling intramolecular electron transfer in complexes with the donor and acceptor connected via flexible linkers. Solution studies have utilized micelles,[15−18] cyclodextrins,[16,19−22] liquid crystals,[23−25] vesicles,[26−28] and lipid bilayers.[29,30]

In this study we have investigated the role of DNA as

† Phone: 404-651-3908. Fax: 404-651-1416. E-mail: ddixon@gsu.edu.

(1) Fox, M. A.; Chanon, M. *Photoinduced Electron Transfer*; Elsevier: Amsterdam, 1988.
(2) Bowler, B. E.; Raphael, A. L.; Gray, H. B. *Prog. Inorg. Chem.* **1990**, *38*, 259−322.
(3) Balzani, V. *Tetrahedron* **1992**, *48*, 10443−10514.
(4) Wasielewski, M. R. *Chem. Rev.* **1992**, *92*, 435−461.
(5) Gust, D.; Moore, T. A.; Moore, A. L. *Acc. Chem. Res.* **1993**, *26*, 198−205.
(6) Kavarnos, G. J. *Fundamentals of Photoinduced Electron Transfer*; VCH: New York, 1993.
(7) Paddon-Row, M. N. *Acc. Chem. Res.* **1994**, *27*, 18−25.
(8) Kurreck, H.; Huber, M. *Angew. Chem., Int. Ed. Engl.* **1995**, *34*, 849−866.
(9) Harriman, A.; Sauvage, J. P. *Chem. Soc. Rev.* **1996**, *25*, 41−48.
(10) Isied, S. S. *Adv. Chem. Ser.* **1997**, *253*, 331−347.
(11) Mataga, N.; Miyasaka, H. *Prog. React. Kinet.* **1997**, *19*, 317−430.
(12) Kakitani, T.; Matsuda, N.; Yoshimori, A.; Mataga, N. *Prog. React. Kinet.* **1997**, *20*, 347−381.
(13) Bixon, M.; Jortner, J. *Adv. Chem. Phys.* **1999**, *106*, 35−202.
(14) Mataga, N.; Miyasaka, H. *Adv. Chem. Phys.* **1999**, *107*, 431−496.
(15) Guindy, N. M.; Elzawawy, F. M.; Sabry, D. Y. *Collect. Czech. Chem. Commun.* **1992**, *57*, 26−32.
(16) Yonemura, H.; Nakamura, H.; Matsuo, T. *Chem. Phys.* **1992**, *162*, 69−78.
(17) Nakamura, H.; Usui, S.; Matsuda, Y.; Matsuo, T.; Maeda, K.; Azumi, T. *J. Phys. Chem.* **1993**, *97*, 534−536.
(18) Szelinski, H.; Niethammer, D.; Tian, P. Z.; Kurreck, H. *Tetrahedron* **1996**, *52*, 8497−8516.
(19) Yonemoto, E. H.; Saupe, G. B.; Schmehl, R. H.; Hubig, S. M.; Riley, R. L.; Iverson, B. L.; Mallouk, T. E. *J. Am. Chem. Soc.* **1994**, *116*, 4786−4795.
(20) Fujiwara, Y.; Aoki, T.; Yoda, K.; Cao, H.; Mukai, M.; Haino, T.; Fukazawa, Y.; Tanimoto, Y.; Yonemura, H.; Matsuo, T.; Okazaki, M. *Chem. Phys. Lett.* **1996**, *259*, 361−364.
(21) Park, J. W.; Lee, B. A.; Lee, S. Y. *J. Phys. Chem. B* **1998**, *102*, 8209−8215.
(22) Yonemura, H.; Kusano, S.; Matsuo, T.; Yamada, S. *Tetrahedron Lett.* **1998**, *39*, 6915−6918.
(23) Levanon, H.; Hasharoni, K. *Prog. React. Kinet.* **1995**, *20*, 309−346.
(24) Elger, G.; Kurreck, H.; Wiehe, A.; Johnen, E.; Fuhs, M.; Prisner, T.; Vrieze, J. *Acta Chem. Scand.* **1997**, *51*, 593−601.
(25) Wiederrecht, G. P.; Svec, W. A.; Wasielewski, M. R. *J. Phys. Chem. B* **1999**, *103*, 1386−1389.
(26) Nakamura, H.; Motonaga, A.; Ogata, T.; Nakao, S.; Nagamura, T.; Matuso, T. *Chem. Lett.* **1986**, 1615−1618.
(27) Otsuki, J.; Ogawa, H.; Okuda, N.; Araki, K.; Seno, M. *Bull. Chem. Soc. Jpn.* **1997**, *70*, 2077−2084.
(28) Otsuki, J.; Okuda, N.; Amamiya, T.; Araki, K.; Seno, M. *J. Chem. Soc., Chem. Commun.* **1997**, 311−312.
(29) Lahiri, J.; Fate, G. D.; Ungashe, S. B.; Groves, J. T. *J. Am. Chem. Soc.* **1996**, *118*, 2347−2358.
(30) Steinberg-Yfrach, G.; Liddell, P. A.; Hung, S. C.; Moore, A. L.; Gust, D.; Moore, T. A. *Nature* **1997**, *385*, 239−241.

10.1021/ic971446s CCC: $18.00
Published on Web 11/10/1999

scaffolding in controlling intramolecular electron transfer. In particular, we have investigated forward electron transfer in a covalently linked donor−acceptor pair both when the molecule is free in solution and when the acceptor portion of the molecule is intercalated into duplex DNA. These studies complement others[31−39] including those of electron transfer between two molecules intercalated into DNA,[37,38,40−46] between a donor at one end of the DNA duplex and an acceptor at the other,[37,38,47−49] and between a donor/acceptor in solution and its electron transfer partner intercalated into DNA.[37,38,46,50−53] They also extend our recent work investigating DNA as a scaffolding for electron transfer between a ferrocene and a covalently appended porphyrin.[54]

The complex in this work consists of a $Ru(bpy)_2(bpy\text{-}CONH\text{-})^{2+}$ (bpy = 2,2′-bipyridine) donor covalently attached by way of a $CH_2CH_2CH_2$ linker to a naphthalene diimide (NDI) acceptor, Ru−NDI, **1**. The $Ru(bpy)_2(bpy\text{-}CONHBu)^{2+}$ model complex, **2**, was studied as well. Tris-bipyridyl ruthenium derivatives are widely used as donors in studies of intramolecular electron transfer.[55−60] They possess outstanding synthetic and photophysical properties. They have a long-lived metal-to-ligand charge transfer (MLCT) state that is strongly emissive; in addition, they are stable in aqueous solution and reversibly photooxidized in the presence of suitable acceptors. Naphthalene diimides, in addition to being good electron acceptors,[61−72] are known to intercalate into double-stranded DNA.[73−78]

Experimental Section

General. *N*-Boc-1,3-diaminopropane (Boc = *tert*-butoxycarbonyl) was purchased from Fluka; *cis*-(2,2′-bipyridine)dichlororuthenium was purchased from ALFA. All other reagents were obtained from Aldrich. Dry dimethylformamide (DMF) was used as received from Aldrich. Neutral alumina (150 mesh, Brockman I, Aldrich) was deactivated by adding 6% water before use in chromatography of the metal complexes. 2,2′-Bipyridine-5-carboxylic acid was prepared according to the literature procedure.[79,80] ^{1}H NMR spectra were taken on Varian Unity+ 500 and 600 MHz spectrometers. FAB spectra were run on a JEOL JMS-SX102/102A/E mass spectrometer using a *m*-nitrobenzyl alcohol matrix. Capillary zone electrophoresis experiments were performed using a Beckman PACE 5510 instrument equipped with a fused-silica capillary (57 cm × 75 μm i.d.) and P/ACE diode array detector. Electrophoresis was performed at a voltage of 13 kV. The sample was introduced into the capillary by high-pressure injection for 5 s. A solution of 50 mM sodium phosphate, pH 2.06 was used as the buffer electrolyte. Product integrations were performed using the Beckman software with absorbance data taken at 450 nm.

The buffer employed was 2.5 mM Na_2HPO_4, 7.5 mM NaH_2PO_4, 0.1 M NaCl, pH 6.5. Calf thymus DNA (CT-DNA, Worthington) was prepared as previously described.[81] Fresh samples were prepared and used immediately before all spectroscopic measurements. Concentrations of DNA are given in base pairs in all experiments based on a molar absorption coefficient of 6600 M^{-1} cm^{-1} per phosphate at 260 nm.[82] Synthesis of the model compound **2** will be reported elsewhere.[83]

Molecular modeling was performed using Sybyl 6.1, Tripos Associates, St. Louis, MO. The coordinates for $Ru(bpy)_3^{2+}$ were taken from the crystal structure.[84]

***N*-3-Aminopropyl-*N*′-3-dimethylaminopropyl-1,4,5,8-naphthalenetetracarboxylic Diimide.** A mixture of 1,4,5,8-naphthalenetetra-

(31) Kirsch-De Mesmaeker, A.; Lecomte, J. P.; Kelly, J. M. *Top. Curr. Chem.* **1996**, *177*, 25−76.
(32) Meade, T. J. *Metal Ions Biol. Syst.* **1996**, *32*, 453−478.
(33) Beratan, D. N.; Priyadarshy, S.; Risser, S. M. *Chem. Biol.* **1997**, *4*, 3−8.
(34) Carter, P. J.; Ciftan, S. A.; Sistare, M. F.; Thorp, H. H. *J. Chem. Educ.* **1997**, *74*, 641−645.
(35) Netzel, T. L. *J. Chem. Educ.* **1997**, *74*, 646−651.
(36) Netzel, T. L. *J. Biol. Inorg. Chem.* **1998**, *3*, 210−214.
(37) Holmlin, R. E.; Dandliker, P. J.; Barton, J. K. *Angew. Chem., Int. Ed. Engl.* **1997**, *36*, 2714−2730.
(38) Kelley, S. O.; Barton, J. K. *Metal Ions Biol. Syst.* **1999**, *36*, 211−249.
(39) Barbara, P. F.; Olson, E. J. C. *Adv. Chem. Phys.* **1999**, *107*, 647−676.
(40) Davis, L. M.; Harvey, J. D.; Baguley, B. C. *Chem.-Biol. Interact.* **1987**, *62*, 45−58.
(41) Brun, A. M.; Harriman, A. *J. Am. Chem. Soc.* **1992**, *114*, 3656−3660.
(42) Stemp, E. D. A.; Barton, J. K. *Metal Ions Biol. Syst.* **1996**, *33*, 325−365.
(43) Franklin, S. J.; Treadway, C. R.; Barton, J. K. *Inorg. Chem.* **1998**, *37*, 5198−5210.
(44) Lincoln, P.; Tuite, E.; Nordén, B. *J. Am. Chem. Soc.* **1997**, *119*, 1454−1455.
(45) Olson, E. J. C.; Hu, D. H.; Hormann, A.; Barbara, P. F. *J. Phys. Chem. B* **1997**, *101*, 299−303.
(46) Harriman, A. *Angew. Chem., Int. Ed.* **1999**, *38*, 945−949.
(47) Murphy, C. J.; Arkin, M. R.; Jenkins, Y.; Ghatlia, N. D.; Bossmann, S. H.; Turro, N. J.; Barton, J. K. *Science* **1993**, *262*, 1025−1029.
(48) Kelley, S. O.; Barton, J. K. *Chem. Biol.* **1998**, *5*, 413−425.
(49) Meade, T. J.; Kayyem, J. F. *Angew. Chem., Int. Ed. Engl.* **1995**, *34*, 352−354.
(50) Fromherz, P.; Rieger, B. *J. Am. Chem. Soc.* **1986**, *108*, 5361−5362.
(51) Dunn, D. A.; Lin, V. H.; Kochevar, I. E. *Biochemistry* **1992**, *31*, 11620−11625.
(52) Atherton, S. J.; Beaumont, P. C. *J. Phys. Chem.* **1995**, *99*, 12025−12029.
(53) Schulman, L. S.; Bossmann, S. H.; Turro, N. J. *J. Phys. Chem.* **1995**, *99*, 9283−9292.
(54) Thornton, N. B.; Wojtowicz, H.; Netzel, T.; Dixon, D. W. *J. Phys. Chem. B* **1998**, *102*, 2101−2110.
(55) Juris, A.; Balzani, V.; Barigelletti, F.; Campagna, S.; Belser, P.; von Zelewsky, A. *Coord. Chem. Rev.* **1988**, *84*, 85−277.
(56) Meyer, T. J. *Acc. Chem. Res.* **1989**, *22*, 163−170.
(57) Hoffman, M. Z.; Bolletta, F.; Moggi, L.; Hug, G. L. *J. Phys. Chem. Ref. Data* **1989**, *18*, 219−543.
(58) Kalyanasundaram, K. *Photochemistry of Polypyridine and Porphyrin Complexes*; Academic Press: London, 1992.
(59) Winkler, J. R.; Gray, H. B. *Chem. Rev.* **1992**, *92*, 369−379.
(60) Durham, B.; Millett, F. *J. Chem. Educ.* **1997**, *74*, 636−640.
(61) Viehbeck, A.; Goldberg, M. J.; Kovac, J. *J. Electrochem. Soc.* **1990**, *137*, 1460−1466.
(62) Green, S.; Fox, M. A. *J. Phys. Chem.* **1995**, *99*, 14752−14757.
(63) Miller, L. L.; Mann, K. R. *Acc. Chem. Res.* **1996**, *29*, 417−423.
(64) Aveline, B. M.; Matsugo, S.; Redmond, R. W. *J. Am. Chem. Soc.* **1997**, *119*, 11785−11795.
(65) Barros, T. C.; Brochsztain, S.; Toscano, V. G.; Berci, P.; Politi, M. J. *J. Photochem. Photobiol. A* **1997**, *111*, 97−104.
(66) Hossain, M. D.; Haga, M.; Monjushiro, H.; Gholamkhass, B.; Nozaki, K.; Ohno, T. *Chem. Lett.* **1997**, 573−574.
(67) Staab, H. A.; Zhang, D. Q.; Krieger, C. *Liebigs Ann./Recl.* **1997**, 1551−1556.
(68) Tan, Q.; Kuciauskas, D.; Lin, S.; Stone, S.; Moore, A. L.; Moore, T. A.; Gust, D. *J. Phys. Chem. B* **1997**, *101*, 5214−5223.
(69) Levanon, H.; Galili, T.; Regev, A.; Wiederrecht, G. P.; Svec, W. A.; Wasielewski, M. R. *J. Am. Chem. Soc.* **1998**, *120*, 6366−6373.
(70) Osuka, A.; Yoneshima, R.; Shiratori, H.; Okada, T.; Taniguchi, S.; Mataga, N. *Chem. Commun.* (*Cambridge*) **1998**, 1567−1568.
(71) Sessler, J. L.; Brown, C. T.; O'Connor, D.; Springs, S. L.; Wang, R. Z.; Sathiosatham, M.; Hirose, T. *J. Org. Chem.* **1998**, *63*, 7370−7374.
(72) Rogers, J. E.; Kelly, L. A. *J. Am. Chem. Soc.* **1999**, *121*, 3854−3861.
(73) Yen, S.-F.; Gabbay, E. J.; Wilson, W. D. *Biochemistry* **1982**, *21*, 2070−2076.
(74) Tanious, F. A.; Yen, S.-F.; Wilson, W. D. *Biochemistry* **1991**, *30*, 1813−1819.
(75) Liu, Z.-R.; Hecker, K. H.; Rill, R. L. *J. Biomol. Struct. Dyn.* **1996**, *14*, 331−339.
(76) Lokey, R. S.; Kwok, Y.; Guelev, V.; Pursell, C. J.; Hurley, L.; Iverson, B. L. *J. Am. Chem. Soc.* **1997**, *119*, 7202−7210.
(77) Bevers, S.; O'Dea, T. P.; McLaughlin, L. W. *J. Am. Chem. Soc.* **1998**, *120*, 11004−11005.
(78) Takenaka, S.; Uto, Y.; Saita, H.; Yokoyama, M.; Kondo, H.; Wilson, W. D. *Chem. Commun.* (*Cambridge*) **1998**, 1111−1112.
(79) Kröhnke, F. *Angew. Chem., Int. Ed. Engl.* **1963**, *2*, 380−393.
(80) Huang, T. L. J.; Brewer, D. G. *Can. J. Chem.* **1981**, *59*, 1689−1700.
(81) Davidson, M. W.; Griggs, B. G.; Boykin, D. W.; Wilson, W. D. *J. Med. Chem.* **1977**, *20*, 1117−1122.
(82) Mahler, H. R.; Kline, B.; Mehrota, B. D. *J. Mol. Biol.* **1964**, *9*, 801−811.
(83) Steullet, V.; Dixon, D. W. *J. Chem. Soc., Perkin Trans. 2*, in press.
(84) Rillema, D. P.; Jones, D. S.; Woods, C.; Levy, H. A. *Inorg. Chem.* **1992**, *31*, 2935−2938.

carboxylic dianhydride (0.27 g, 1.0 mmol), *N*-Boc-1,3-diaminopropane (170 mg, 1.0 mmol), and *N*,*N*-dimethyl-1,3-diaminopropane (110 mg, 1.0 mmol) in toluene (100 mL) was stirred and refluxed with a Dean Stark receiver for 3 h. The reaction mixture was evaporated and purified by silica gel chromatography with use of gradient elution (100% EtOAc, 10% EtOAc/$CHCl_3$). The second band was collected, evaporated, dissolved in trifluoroacetic acid, allowed to stand for 1 h, and evaporated. The residue was dissolved in hot water (50 mL) and washed with $CHCl_3$ (3 × 20 mL). The water solution was evaporated to dryness to obtain product, which NMR showed to be pure (92 mg, 15%). ^{1}H NMR (D_2O, 25 °C): δ 1.95 (m, 2H, CH_2CH$_2$N), 2.05 (m, 2H, CH_2-CH$_2$N), 2.78 (s, 6H, CH_3), 2.99 (t, 2H, CH_2NH$_2$), 3.18 (t, 2H, CH_2N-(CH$_3$)$_2$), 4.07 (m, 4H, CH_2ar), 8.22 (s, 4H, ar).

***N*-3-(2,2′-Bipyridine-5-carboxamide)propyl-*N*′-3-dimethylaminopropyl-1,4,5,8-naphthalenetetracarboxylic Diimide.** *N*-3-Aminopropyl-*N*′-3-dimethylaminopropyl-1,4,5,8-naphthalenetetracarboxylic diimide (110 mg, 0.17 mmol), 2,2′-bipyridine-5-carboxylic acid (42 mg, 0.21 mmol), benzotriazol-1-yloxy-tris(dimethylamino)phosphonium hexafluorophosphate (BOP) (110 mg, 0.25 mmol), and triethylamine (100 mg, 1.0 mmol) were mixed in dry DMF (10 mL). The mixture was stirred for 1 day at room temperature. The solution was evaporated, washed with hot methanol, filtered, and dried to give product, which NMR showed to be pure (50 mg, 42%). ^{1}H NMR (DMSO, 30 °C): δ 2.01 (m, 4H, CH_2CH$_2$N), 2.72 (s, 6H, CH_3), 3.05 (t, 2H, CH_2NH), 3.41 (m, 2H, CH_2N(CH$_3$)$_2$), 4.12 (t, 2H, CH_2ar), 4.19 (t, 2H, CH_2ar), 7.52 (t, 1H, Py), 7.99 (t, 1H, Py), 8.26 (d, 1H, Py), 8.40 (d, 2H, Py), 8.67 (s, 4H, ar), 8.71 (d, 1H, Py), 8.79 (t, 1H, Py), 9.05 (s, 1H, NHCO).

[Ru(bipyridine)$_2$(L)Cl$_2$] (L = *N*-3-(2,2′-Bipyridine-5-carboxamide)propyl-*N*′-3-dimethylaminopropyl-1,4,5,8-naphthalenetetracarboxylic Diimide) (1). *N*-3-(2,2′-Bipyridine-5-carboxamide)propyl-*N*′-3-dimethylaminopropyl-1,4,5,8-naphthalenetetracarboxylic diimide (20 mg, 0.034 mmol) dissolved in 10 mL of DMF was added to *cis*-(2,2′-bipyridine)dichlororuthenium(II) dihydrate (78 mg, 0.15 mmol) dissolved in 15 mL of hot water. The solution was deaerated with nitrogen for 20 min and then heated and refluxed for 3 h under nitrogen. The reaction mixture was evaporated, and the residue was dissolved in acetonitrile and purified by an alumina column with use of gradient elution (100% CH_3CN, 10%MeOH/CH_3CN). The second orange band was collected and evaporated to give product (12 mg, 33%). ^{1}H NMR (CD_3CN, 25 °C): δ 2.41 (t, 2H, CH_2NH), 3.30 (s, 6H, CH_3), 3.35 (t, 2H, CH_2N(CH$_3$)$_2$), 4.08 (t, 2H, CH_2ar), 4.20 (t, 2H, CH_2ar), 7.40−7.47 (m, 5H, Py), 7.70−7.78 (m, 3H, Py), 7.94−8.12 (m, 7H, Py), 8.32 (s, 1H, Py), 8.53−8.78 (m, 11H, Py, ar), 9.46 (t, 1H, NHCO). FAB-MS: *m*/*z* 1004.76 (M^+ calcd 1004.27 for $C_{53}H_{46}N_{10}O_5Ru$, presumably reduced in situ). CE: 12.44 min retention time (CE = capillary electrophoresis).

UV−Visible Absorption. UV−visible absorption spectra were obtained on either a Perkin-Elmer Lambda-6 or a Shimadzu UV-3101PC spectrophotometer using 1 nm bandwidths. The concentrations of solutions of **1** and Ru(bpy)$_3$Cl$_2$ were determined using the molar absorption coefficients (ϵ) at 450 nm (for **1** in buffer ϵ_{450} = 12 400 M^{-1} cm^{-1};[85] and for Ru(bpy)$_3$Cl$_2$ in buffer ϵ_{450} = 14 600 M^{-1} cm^{-1}).[86] Concentrations of solutions of NDI−(NR$_2$)$_2$ were determined from the molar absorption coefficients at 383 nm (in buffer ϵ_{383} = 31 000 M^{-1} cm^{-1}). For UV−visible DNA titrations, small volumes of a concentrated DNA solution of known concentration were added via syringe to a 3 mL volume of the compound in buffer solution (typically 2−3 × 10^{-5} M in compound); the solution was mixed by repeated inversion and its absorption measured approximately 15 min afterward. Waiting longer times after DNA addition did not appreciably affect the absorption spectra.

Circular dichroism (CD) measurements were performed on a Jasco J-600 spectropolarimeter using quartz cuvettes and a 1 nm bandwidth. Optical densities of the samples were approximately 0.8−1.0 at 383 nm. The spectra were normalized to molar units by dividing the number of millidegrees by the sample molar concentrations.

Steady State Fluorescence. Fluorescence spectra were recorded on either SLM-8000C (SLM Aminco, Inc.) or PTI QM-1 (Photon Technology International, Inc., QuantaMaster) spectrofluorometers. All spectra were corrected for the wavelength-dependent emission response of each spectrofluorometer, and spectra recorded on either system agreed with spectra recorded on the other. To eliminate artifacts due to polarized emission, the SLM system depolarized the excitation light with an achromatic depolarizer before it entered the sample cell and collected the emission through a film polarizer set at 54.7° with respect to vertical. The PTI system used a pair of calcite polarizers and vertically polarized the excitation light, while collecting the emission through the second polarizer set at 54.7° with respect to vertical. Sample absorbances at the excitation wavelength (460 nm) were typically less than or equal to 0.15. Relative emission quantum yields (Φ_{em}) were determined with respect to air-saturated water according to the following equation:

$$\Phi_{em} = [\Phi_{em}^{s}/\Phi_{em}^{r}] = [(Q_s/A_s)/(Q_r/A_r)](\eta_S/\eta_R)^2 \qquad (1)$$

where the s and r sub- and superscripts refer respectively to solutions of the unknown sample and the reference compound, Ru(bpy)$_3$Cl$_2$; A is the solution's absorbance at the excitation wavelength; Q is the number of emission quanta, obtained by integrating a wavelength- and quanta-corrected emission spectrum; and η is the index of refraction of the solvent.

Fluorescence Lifetime Measurements. Fluorescence decays were recorded on a Tektronix SCD1000 transient digitizer (≤0.35 ns rise time calculated from the bandwidth, ≤120 ps rise time for a step input 0.5 times the vertical range). Emission was detected with a Hamamatsu 1564U microchannel plate (200 ps rise time) after passing through a Hoya 058 sharp-cut glass filter to eliminate scattered excitation light at 532 nm. The excitation and emission beams were oriented at 90° with respect to each other as in the steady state fluorescence experiments. To eliminate rotational diffusion artifacts, Glan-Thompson calcite polarizers were inserted in the excitation and emission beams and set as in the PTI QM-1 system described above.[87] The 532 nm excitation light for emission decay measurements was generated as the second harmonic of an active−passive mode-locked Nd^{3+}/YAG laser manufactured by Continuum, Inc. Typically 30−35 μJ excitation pulses of ca. 25 ps duration were collimated into a 5 mm diameter beam before entering the sample cuvette. PTI software, specially modified by the manufacturer to process 1000 data points per decay curve, was used to reconvolute iteratively the detection system's instrument response and trial exponential decay functions until a best fit to the actual emission decay was obtained. Goodness of fit was judged by a minimized reduced χ^2 statistic (χ_r^2) and randomly distributed residual errors. Samples were contained in rectangular quartz cuvettes at concentrations of ca. 2 × 10^{-5} M.

The general temporal resolution of the emission kinetics system for multiexponential decays is ca. 0.2 ns. A detailed description of the lifetime fitting procedure used here is presented in a recent paper by Netzel and co-workers[88] for nine sets of emission decays on four time scales (20, 50, 100, and 500 ns) and includes the following: the equations used; plots of residual differences between experimental emission decays and calculated multiexponential curves; linear and logarithmic plots of emission decays, lamp decays, and exponential curves; as well as χ_r^2 values for the plotted best-fit curves.

Results

Synthesis. The Ru−NDI compound **1** was synthesized by initial condensation of 1,4,5,8-naphthalenetetracarboxylic dianhydride with equimolar amounts of *N*-Boc-1,3-diaminopropane and *N*,*N*-dimethyl-1,3-diaminopropane (Figure 1). The

(85) Belser, P.; von Zelewsky, A.; Frank, M.; Seel, C.; Vögtle, F.; De Cola, L.; Barigelletti, F.; Balzani, V. *J. Am. Chem. Soc.* **1993**, *115*, 4076−4086.

(86) Pyle, A. M.; Rehmann, J. P.; Meshoyrer, R.; Kumar, C. V.; Turro, N. J.; Barton, J. K. *J. Am. Chem. Soc.* **1989**, *111*, 3051−3058.

(87) Lakowicz, J. R. *Principles of Fluorescence Spectroscopy*; Plenum Press: New York, 1986.

(88) Manoharan, M.; Tivel, K. L.; Zhao, M.; Nafisi, K.; Netzel, T. L. *J. Phys. Chem.* **1995**, *99*, 17461−17472.

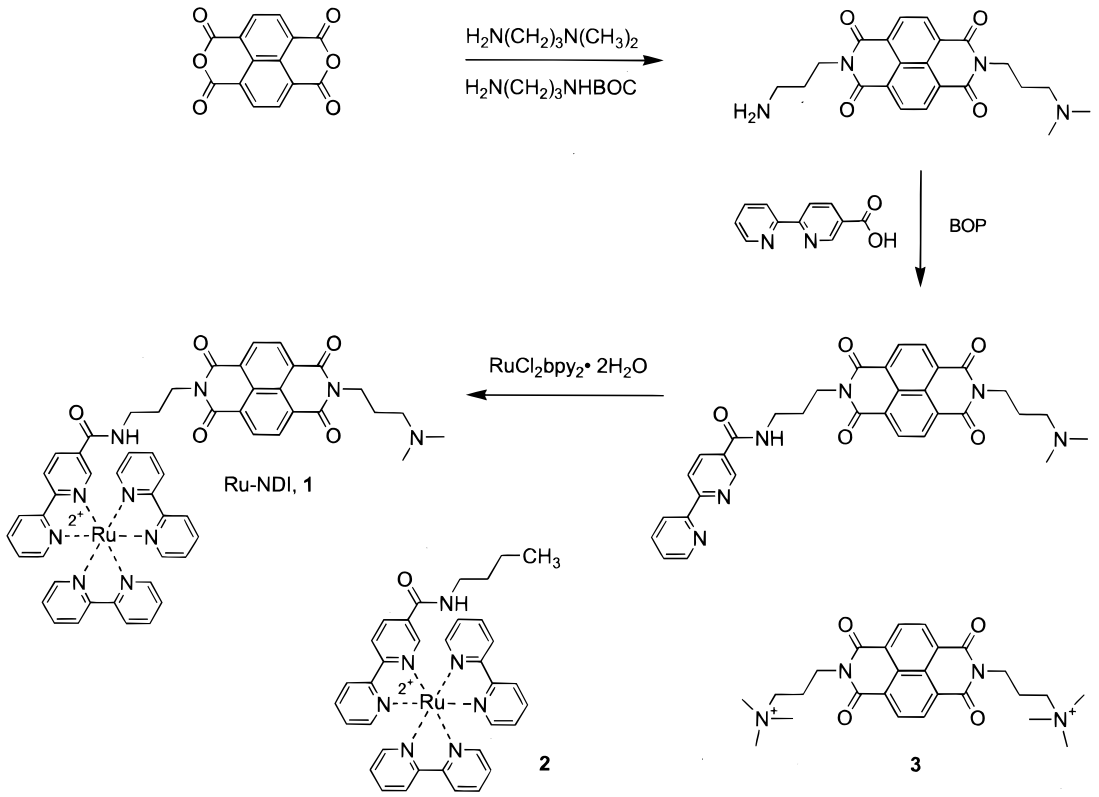

Figure 1. Synthetic scheme for the preparation of Ru−NDI **1**; structures of **2** and **3**.

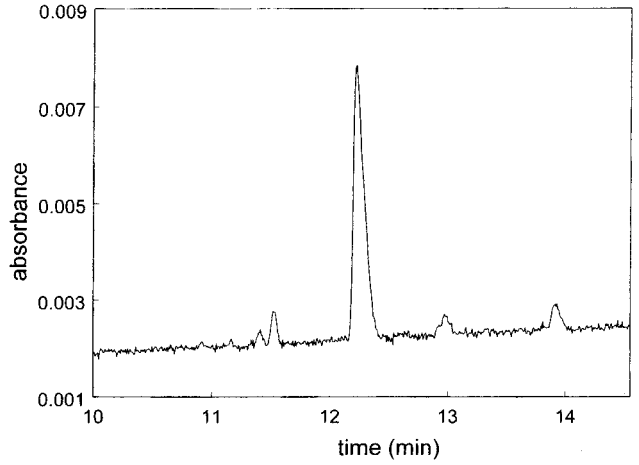

Figure 2. Capillary electrophoresis of **1** using a fused-silica capillary (57 cm × 75 μm i.d.); a solution of 50 mM sodium phosphate, pH 2.06 was used as the buffer electrolyte. The larger impurity peak before the main peak is $Ru(bpy)_3^{2+}$.

product was separated by silica gel chromatography with use of gradient elution. The Boc group was removed with trifluoroacetic acid, and the resulting primary amine was condensed with 2,2′-bipyridine-5-COOH using BOP as a coupling agent. This was allowed to react with excess $Ru(bpy)_2Cl_2$, and the product was purified by chromatography on neutral alumina with use of gradient elution.

Capillary electrophoresis proved to be useful in analyzing the purity of this compound. Excellent separations were achieved in uncoated fused-silica capillaries with a 50 mM sodium phosphate, pH 2.06 buffer. Figure 2 shows a representative chromatograph. Co-injection with an authentic sample of $Ru(bpy)_3^{2+}$ indicated that the peak (6% of the total area) coming before the main peak was $Ru(bpy)_3^{2+}$. Peaks coming after the main peak contained both ruthenium−bipyridine and NDI moieties, as evidence by their optical spectra (diode array detection). It should be noted that the $Ru(bpy)_3^{2+}$ moiety is intrinsically chiral. No effort was made to separate the enantiomers in the mixture.

Because the spectral characteristics of the $Ru(bpy)_3^{2+}$ moiety are controlled in part by the substituents on the bipyridine rings, we also synthesized a ruthenium complex with two unsubstituted bipyridine rings and the third bearing an amide at the 5-position on one of the rings, the $Ru(bpy)_2(bpy\text{-}CONH\text{-}butyl)^{2+}$ complex, **2**. To evaluate the intercalation of the diimide group in **1**, we also made the known diimide **3** with symmetrical CH_2CH_2-$CH_2N^+Me_3$ side chains.[83,89]

One of the issues in studying donor−linker−acceptor molecules with linkers which are not rigid is the relative geometries of the donor and acceptor. Some indication of this for **1** in water is given by the NMR spectrum of this compound in comparison with that of **2**. Compounds **1** and **2** each have 23 inequivalent bipyridine protons, eight each in the two unsubstituted rings and seven in the substituted ring. In the ^{1}H NMR spectrum, these are seen as a series of multiplets in the 7.3−8.7 ppm region. Each of the multiplets has a larger chemical shift range in **1** than in the model **2**. For example the 4-H protons (para to the pyridine nitrogen in each ring) have a chemical shift range of 0.16 ppm in compound **1** and 0.08 ppm in the model **2**. This is ascribed to small differences in the shielding experienced by the protons in the bipyridine rings of **1** due to geometries in which the bipyridine rings lie in the shielding cone of the NDI moiety. Another indication that the Ru−bipyridine system lies at least in part over the NDI moiety is that the ring protons of the NDI ring itself are not seen as a singlet. Although the NDI ring protons are not formally equivalent because the side chains are not the same, these ring protons might have been expected to be observed as a singlet because the chain termini [NMe_2

(89) Zhong, C. J.; Kwan, W. S.; Miller, L. L. *Chem. Mater.* **1992**, *4*, 1423−1428.

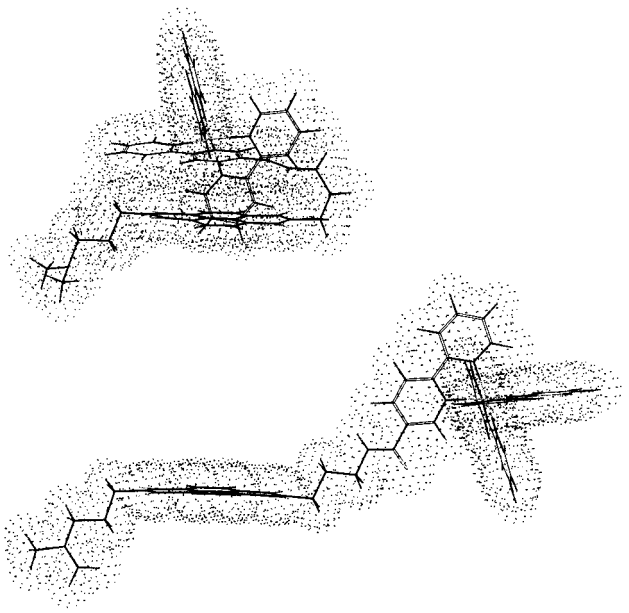

Figure 3. Possible conformations of **1** in solution.

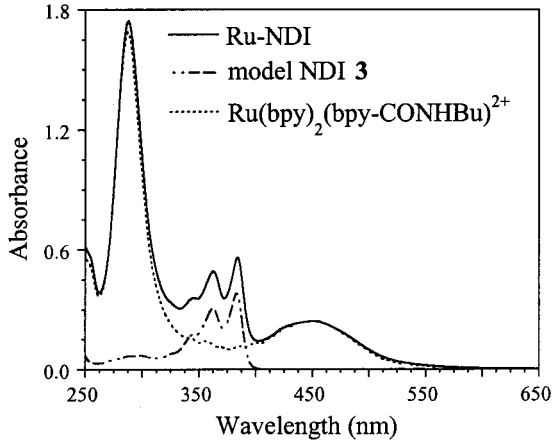

Figure 4. Overlay of UV−visible absorbance spectra for Ru−NDI **1**, **2** [$Ru(bpy)_2$−(bpy-$CONHBu)^{2+}$] and model NDI **3** [NDI−($CH_2CH_2CH_2N^+Me_3)_2$] in buffer. The spectra of **1** and **2** were normalized to one another at 450 nm.

and $Ru(bpy)_2(bpy\text{-}CONH)^{2+}$] are insulated from the central NDI ring by three methylene units on each side (the precursor NDI with $CH_2CH_2CH_2NMe_2$ and $CH_2CH_2CH_2NHCO$-bipyridine side chains showed a singlet in the NMR for the NDI ring protons). Figure 3 shows two limiting geometries for **1**, one fully extended and one in which one of the bipyridine rings is closely associated with the NDI moiety.

UV−Visible Absorbance Spectra. The absorbance spectrum of **1** is a composite of the absorbance spectra from both the NDI moiety and the $Ru(bpy)_2(bpy\text{-}CONH)^{2+}$ metal complex, as illustrated in the overlay of the UV−visible absorbance spectra of the model compounds [$Ru(bpy)_2(bpy\text{-}CONHBu)^{2+}$ **2** and **3**] and **1** all in buffer (Figure 4). The visible region (400−550 nm) for **1** consists of the characteristic Ru ($d\pi$) → bpy (π^*) metal-to-ligand charge transfer (MLCT) transition;[55] the peaks at 383 and 362 nm are mainly due to π,π^* transitions in NDI with some contribution from underlying MLCT absorbance. At higher energies the peaks correspond to ligand-centered transitions from both components. The MLCT band for **1** is broadened and shifted slightly to the red in comparison to $Ru(bpy)_3^{2+}$. This is likely a consequence of the presence of two types of MLCT transitions within the complex: Ru* → bpy and Ru* → bpy-CONHR. The amido substituent on one bpy ligand is electron-withdrawing, resulting in a lower π^* level for this ligand relative to the two unsubstituted bpy ligands on the complex.[85,90]

Steady State Emission and Lifetimes. Excitation of **1** at 460 nm results in an emission spectrum with a maximum at 626 (±4) nm. This is essentially the same maximum emission wavelength as that of $Ru(bpy)_3^{2+}$ [624 (±4) nm]. The model compound **2** has its emission maximum in aqueous buffer at 674 (±4) nm. For comparison purposes it is worth noting that a compound closely related to **2** also has an emission maximum at a longer wavelength than does $Ru(bpy)_3^{2+}$. The compound is $[Ru(2,2'\text{-bipyridine})_2L]^{2+}$, where L = 4′-methyl-2,2′-bipyridyl-4′-carbonyl-$NHCH_3$, with an emission maximum at 645 nm in acetonitrile.[90] Compound **2** lacks a 4′-methyl group on the substituted bipyridyl ligand and has a 5′-carbonyl-NH-butyl group; its emission was measured in water, not acetonitrile. Red-shifted emission (640 nm) relative to $Ru(bpy)_3^{2+}$ (626 nm) has also been reported in acetonitrile for yet another compound closely related to **2**. This compound contains two [$Ru(2,2'\text{-bipyridine})_2L^{2+}$] chromophores each linked to a central anthracene [L = a 2,2′-bipyridinyl-4′-carbonyl-(*N*-benzyl) aminomethyl anthracene]. Taken collectively our emission results for **2** in water and those of the two compounds closely related to **2** in acetonitrile suggest that the 626 nm emission maximum from a sample of **1** in aqueous buffer shows that this sample's steady state emission is dominated by a $Ru(bpy)_3^{2+}$ impurity. That is, the actual emission of **1** should resemble the emission of **2** and be red-shifted relative to that of $Ru(bpy)_3^{2+}$. However, **1**'s emission is much weaker than of the $Ru(bpy)_3^{2+}$ impurity. It is expected that the Ru chromophore in **1** will produce only minimal emission compared to $Ru(bpy)_3^{2+}$ itself, because the MLCT state of **1** should be rapidly quenched by electron transfer to the NDI chromophore. Thus, emission from small amounts (approximately 6% by CE analysis) of unquenched $Ru(bpy)_3^{2+}$ impurity in samples of **1** can easily dominate the sample's steady state emission spectrum. The relative emission quantum yields of **1** in comparison, respectively, to $Ru(bpy)_3^{2+}$ and **2** are 0.053 (±0.002) and 0.35 (±0.04). Note that **2** itself has a reduced emission quantum yield relative to $Ru(bpy)_3^{2+}$ of 0.15 (±0.01).

The emission decay of $Ru(bpy)_3^{2+}$ was measured to be 415 ns in both water and aqueous buffer solutions. This is in good agreement with literature values.[86,91,92] Fitting the emission decay of a solution of **2** in aqueous buffer requires two lifetimes. Approximately 98% of the emission amplitude decays with a lifetime of 70 ns, while the remaining amplitude decays with a lifetime of 415 ns. Because the 415 ns lifetime component is similar to that of $Ru(bpy)_3^{2+}$ itself, it is likely that this long-lived component is also due to a $Ru(bpy)_3^{2+}$ impurity as was suggested above for **1**. If **2** and $Ru(bpy)_3^{2+}$ have similar radiative rates, the ratio of their emission lifetimes (τ) and quantum yields (Φ_{em}) should be similar, and indeed they are: $\tau(\mathbf{2})/\tau(Ru(bpy)_3^{2+}) = 70/415 = 0.17$ and $\Phi_{em}(\mathbf{2}) = 0.15$. Table 1 summarizes all of the emission lifetime and relative emission quantum yield data. It also presents excitation wavelength, emission wavelength, and sample concentration data for the various experiments.

Photophysical Studies in Solution without DNA. The emission decay for **1** in buffer is shown on the 100 ns time scale in Figure 5. The emission decay for **1** was fit to four

(90) Mecklenburg, S. L.; Peek, B. M.; Schoonover, J. R.; McCafferty, D. G.; Wall, C. G.; Erickson, B. W.; Meyer, T. J. *J. Am. Chem. Soc.* **1993**, *115*, 5479−5495.
(91) Kumar, C. V.; Barton, J. K.; Turro, N. J. *J. Am. Chem. Soc.* **1985**, *107*, 5518−5523.
(92) Tossi, A. B.; Kelly, J. M. *Photochem. Photobiol.* **1989**, *49*, 545−556.

Table 1. Emission Lifetimes and Relative Emission Quantum Yields (Φ_{em}) of Ru−NDI[a]

compd	solvent	DNA_{bp}/NDI	(α_1)	τ_1, ns[b]	(α_2)	τ_2, ns	(α_3)	τ_3, ns	$\langle\tau\rangle$, ns[c]	χ_r^2 [d]	Φ_{em}[e]
1	N10[f]	0	(0.88)	0.34 ±0.04	(0.11)	1.99 ±0.18	(0.008)	12.6 ±0.4	0.62 ±0.06	2.0	0.053 ±0.004
	N10:DNA	17	(0.79)	0.31 ±0.06	(0.13)	2.00 ±0.16	(0.08)	11.8 ±0.9	1.45 ±0.14	0.7	0.055 ±0.004
$Ru(bpy)_3^{2+}$	H_2O	0	(1.0)	415 ±5					415 ±5	1.3	1.00
	N10	0	(1.0)	415 ±5					415 ±5	0.5	
	N10:DNA	17	(0.45)	310 ±4	(0.55)	647 ±10			495 ±7	0.2	1.00 ±0.06
2	N10	0	(0.98)	70.0 ±0.8	(0.02)	415 ±20			76 ±1	0.5	0.15 ±0.01
	N10:DNA	17	(0.98)	69.6 ±0.8	(0.02)	420 ±20			77 ±1	0.2	0.14 ±0.01

[a] All emission decays were obtained on freshly prepared samples placed in quartz cuvettes. Samples were typically ca. 4.5×10^{-5} M in concentration and were excited at 532 nm with emission monitored at wavelengths above 580 nm. Analysis of the emission decays for Ru−NDI **1** involved fitting the experimental data to four exponentials, assigning the fourth emission component zero amplitude and normalizing the amplitudes of the three remaining lifetimes to 100%. The fourth decay component had an amplitude of ca. 0.02 and a lifetime on the order of that for unquenched $Ru(bpy)_3^{2+}$; it was attributed to a Ru(II) impurity. [b] α_i represents fractional relative emission amplitudes; τ_i represents lifetime in nanoseconds for each decay component. [c] Average emission lifetimes were calculated according to $\langle\tau\rangle = \sum_i(\alpha_i\tau_i)$ where i is the ith component for the decays, α is the fractional amplitude, and τ is the lifetime for each component. [d] Reduced χ^2 parameter (χ_r^2) indicating the goodness of the fit to the data. [e] All steady state emission quantum yields were determined relative to the emission intensity of $Ru(bpy)_3^{2+}$ in air-saturated H_2O which has a quantum yield of 0.038. Samples were typically 2.3×10^{-5} M in concentration and were excited at 460 nm. [f] N10 is 10 mM phosphate buffer pH 6.5 with 0.1 M NaCl added.

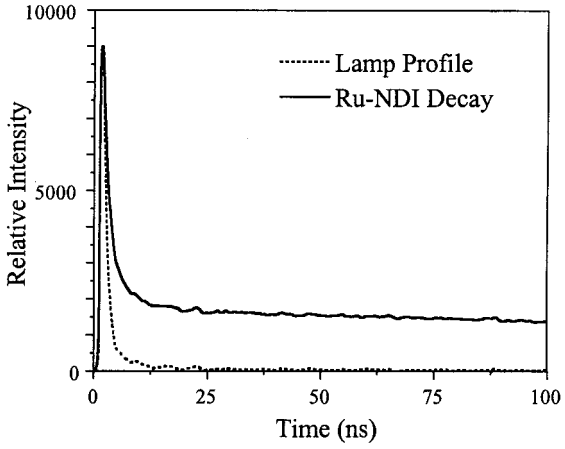

Figure 5. Emission decay on the 100 ns time scale for Ru−NDI **1** [0.045 mM] in air-saturated buffer with excitation at 532 nm and emission monitored >580 nm.

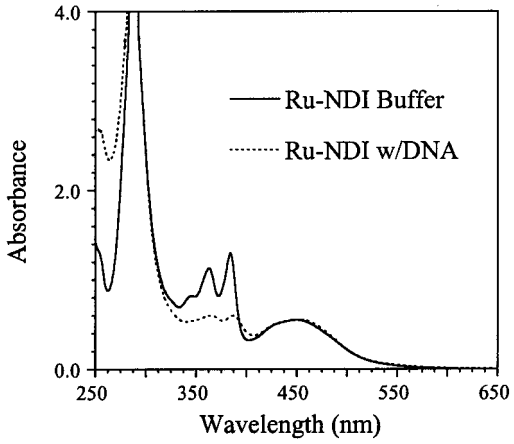

Figure 6. UV−visible absorbance spectra for Ru−NDI **1** [0.044 mM] in buffer in the absence and presence of calf thymus DNA [0.15 mM base pairs].

exponentials resulting in lifetimes of 0.34, 1.99, 12.6, and 360 ns. The longest-lived component had a fractional amplitude (α_i) of 2−3%. Consistent with the capillary electrophoresis and emission spectra described above, this long-lived emission component (τ_4) is ascribed to luminescence from Ru^{II} complexes not covalently linked to an intact NDI quencher. The fractional contribution of τ_4 remained constant throughout the fits and was discarded from the analyses by assigning zero amplitude to τ_4 and renormalizing the amplitudes of $\tau_1-\tau_3$.

Ninety-nine percent of the initial intensity is due to the two short-lived species (τ_1 and τ_2), as evidenced in the sharp drop-off of the decay for **1** in Figure 5. The average emission lifetime ($\langle\tau\rangle$) for **1**, excluding the 360 ns component, is 0.62 (±0.06) ns. Thus the average emission lifetime for **1** is 99% quenched compared to the emission lifetime for **2**. An average rate of quenching, assigned to intramolecular electron transfer ($\langle k_{ET}\rangle$), can be determined using the relationship $\langle k_{ET}\rangle = 1/\langle\tau\rangle - 1/\tau_o$, where $\langle\tau\rangle$ and τ_o are respectively the average emission lifetime of **1** and the lifetime of model **2** (70 ns): $\langle k_{ET}\rangle = 1.6 \times 10^9$ s^{-1}.

DNA Binding. To determine the mode of interaction of **1** with double-stranded DNA, the absorbance characteristics and circular dichroism of **1** in the presence of increasing amounts of calf thymus DNA were examined. In the optical spectrum, signatures of intercalative binding, where the planar aromatic ring system of a molecule inserts itself between the base pairs of the DNA double helix, are hypochromism and red shifts in the long-wavelength absorbance transitions of the intercalated species[93] (hypochromicity, $H\% = [((\epsilon_f - \epsilon_b)/\epsilon_f) \times 100]$ where ϵ_f and ϵ_b are the molar absorption coefficients for free and bound intercalators at λ_f and λ_b nm, respectively). Addition of DNA to buffer solutions of **1**, at DNA base pair (DNA_{bp}) to **1** ratios ≥4, resulted in a 48−52% decrease and approximate 4 nm red shift of the NDI band at 383 nm (Figure 6). This is very similar to the 63% hypochromism and approximate 2 nm red shift observed for NDI bearing $CH_2CH_2CH_2N^+HMe_2$ side chains.[73] The NDI-band hypochromism for **1** bound to DNA reached a plateau at $[DNA_{bp}]/[\mathbf{1}] > 4$; above this ratio, the hypochromism remained essentially constant. Additionally, the MLCT band of **1** was unchanged in both wavelength and absorbance intensity for $[DNA_{bp}]/[\mathbf{1}]$ ratios less than 40 (highest ratio investigated). The binding constant of naphthalene diimides to DNA is

(93) Bloomfield, V. A.; Crothers, D. M.; Tinoco, I., Jr. *Physical Chemistry of Nucleic Acids*; Harper & Row: New York, 1974.

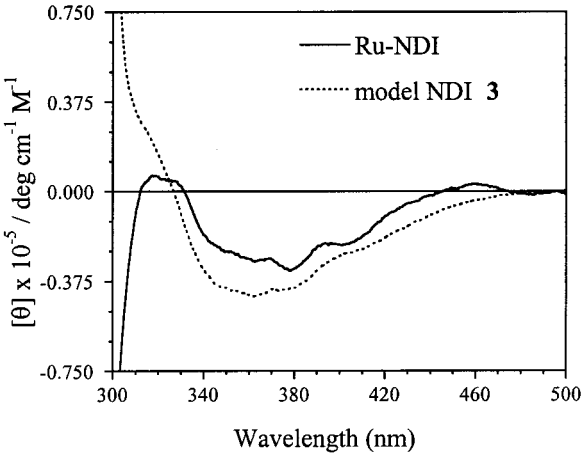

Figure 7. Induced CD spectra of **1** (0.044 mM, $[DNA_{bp}]/[\mathbf{1}] = 17$) and the model NDI **3** (0.058 mM, $[DNA_{bp}]/[\mathbf{1}] = 29$) with DNA.

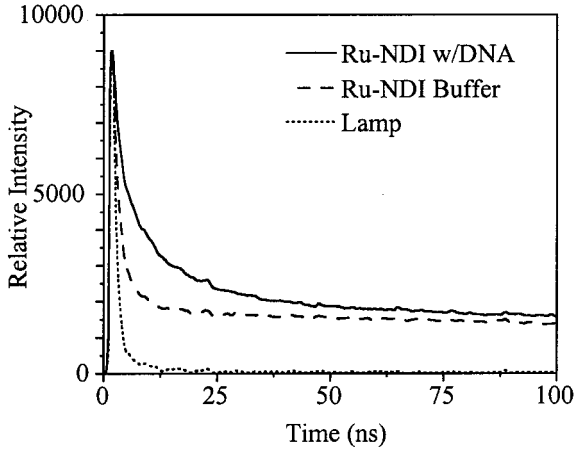

Figure 8. Normalized emission decays on a 100 ns time scale for **1** [0.049 mM] in air-saturated buffer in the absence and presence of calf thymus DNA (0.82 mM base pairs). Excitation was at 532 nm, and emission was monitored at >580 nm.

approximately 5×10^5 M^{-1}.[74] Therefore, for the $[DNA_{bp}]/[NDI]$ ratios of ≥15 used in this study, >99% of the NDI compounds investigated herein would be expected to be bound to the DNA.

The induced CD spectrum of **1** in DNA, at a $[DNA_{bp}]/[\mathbf{1}]$ ratio equal to 17, shows a negative absorption band in the 330−420 nm region that contains modest structural features similar to those in the UV−visible absorption spectrum of **1** in DNA (Figure 7). As expected, **1** does not exhibit a CD spectrum in buffer in the absence of DNA. The induced CD spectrum of **1** in DNA is similar to the induced CD spectrum of the model NDI **3** in DNA, as illustrated in the overlay of their spectra in Figure 7. The similarity of the CD data for **1** and **3** indicates that the NDI moiety in **1** binds to DNA as an intercalator. The Ru moiety in **1** shows little to no induced signal in the CD spectrum, suggesting that it interacts only weakly with the DNA.

Photophysical Studies of Ru−NDI 1 in DNA. Under conditions where $[DNA_{bp}]/[\mathbf{1}] = 17$, the steady state emission quantum yield for **1** is 0.055 (±0.004), approximately the same as its quantum yield in the absence of DNA (Table 1). Using the same fitting procedure as described for **1** in buffer, the emission decay for **1** at $[DNA_{bp}]/[\mathbf{1}] = 17$ is fit to a four-exponential function giving lifetimes of 0.31, 2.00, 11.8, and 390 ns (Figure 8). The renormalized fractional amplitudes (neglecting the 390 ns component) for the first three decay components are $\alpha_1 = 0.79$, $\alpha_2 = 0.13$, and $\alpha_3 = 0.08$. The most significant feature of the decay of **1** in DNA, in comparison to the decay of **1** in buffer (Table 1), is the overall increase in fractional contribution of the two longest-lived emission components and corresponding decrease in the fractional amplitude of the shortest-lived component. The decay of **1** in DNA is still dominated (79%), however, by the shortest-lived emission (310 ps) as it was in buffer. This results in an average emission lifetime for **1** in DNA of 1.45 ns (excluding τ_4) and an average electron transfer rate of 6.8×10^8 s^{-1}.

Discussion

The goal of this work was to compare electron transfer from a donor to a covalently linked acceptor in solution and in DNA scaffolding. As the donor, we chose $Ru(bpy)_3^{2+}$. This chromophore is widely used in supramolecular chemistry because it has excellent photophysical characteristics.[55,56,58] The link was made via the 5-substituted carboxamide derivative, chosen because the bipyridine-5-COOH starting material can be prepared fairly readily via the Kröhnke synthesis.[79,80] In addition, relevant photophysical and electrochemical properties of Ru^{II} tris-bpy complexes that are closely related to the $Ru^{II}(bpy)_2$(bpy-CONHR) moiety in compounds **1** and **2** have been measured by Balzani and co-workers[85] and by Meyer and co-workers.[90] $Ru(bpy)_3^{2+}$ binds in the grooves of DNA.[86,94,95] As the acceptor, we chose the naphthalene diimide ring, which has been used as an electron acceptor previously in donor−acceptor complexes.[66,67,69,71,96−106] The naphthalene diimide ring intercalates in DNA.[73−78] Thus, Ru−NDI **1** was designed as a donor−acceptor complex with excellent photophysical characteristics which would interact in a straightforward manner with DNA.

Photophysical Studies in Solution without DNA. Red shifts in the UV−visible spectra for **1** and **2** compared to the spectrum for $Ru(bpy)_3^{2+}$ indicate slight differences in the energy of the MLCT state of **1** and **2** compared to the MLCT state of $Ru(bpy)_3^{2+}$. This difference is attributable to the electron-withdrawing carboxamido substituent on one of the bpy ligands attached to the metal center of **1** and **2**. As a result, the bpy-CONHR ligand is expected to possess a lower-energy π,π^* transition. The red shifts in the luminescence peaks for **1** and **2** compared to $Ru(bpy)_3^{2+}$ suggest that the excited electron in their MLCT states is localized primarily on the lower-energy bpy-

(94) Scott, J. R.; McLean, M.; Sligar, S. G.; Durham, B.; Millett, F. *J. Am. Chem. Soc.* **1994**, *116*, 7356−7362.
(95) Johnston, D. H.; Thorp, H. H. *J. Phys. Chem.* **1996**, *100*, 13837−13843.
(96) Osuka, A.; Zhang, R.-P.; Maruyama, K.; Ohno, T.; Nozaki, K. *Chem. Lett.* **1993**, 1727−1730.
(97) Osuka, A.; Zhang, R. P.; Maruyama, K.; Mataga, N.; Tanaka, Y.; Okada, T. *Chem. Phys. Lett.* **1993**, *215*, 179−184.
(98) Hasharoni, K.; Levanon, H.; Greenfield, S. R.; Gosztola, D. J.; Svec, W. A.; Wasielewski, M. R. *J. Am. Chem. Soc.* **1995**, *117*, 8055−8056.
(99) Osuka, A.; Marumo, S.; Wada, Y.; Yamazaki, I.; Yamazaki, T.; Shirakawa, Y.; Nishimura, Y. *Bull. Chem. Soc. Jpn.* **1995**, *68*, 2909−2915.
(100) Osuka, A.; Shiratori, H.; Yoneshima, R.; Okada, T.; Taniguchi, S.; Mataga, N. *Chem. Lett.* **1995**, 913−914.
(101) Greenfield, S. R.; Svec, W. A.; Gosztola, D.; Wasielewski, M. R. *J. Am. Chem. Soc.* **1996**, *118*, 6767−6777.
(102) Smirnov, S. N.; Braun, C. L.; Greenfield, S. R.; Svec, W. A.; Wasielewski, M. R. *J. Phys. Chem.* **1996**, *100*, 12329−12336.
(103) Wiederrecht, G. P.; Niemczyk, M. P.; Svec, W. A.; Wasielewski, M. R. *J. Am. Chem. Soc.* **1996**, *118*, 81−88.
(104) Wiederrecht, G. P.; Yoon, B. A.; Svec, W. A.; Wasielewski, M. R. *J. Am. Chem. Soc.* **1997**, *119*, 3358−3364.
(105) Shiratori, H.; Ohno, T.; Nozaki, K.; Yamazaki, I.; Nishimura, Y.; Osuka, A. *Chem. Commun.* (*Cambridge*) **1998**, 1359−1360.
(106) Wiederrecht, G. P.; Wasielewski, M. R. *J. Am. Chem. Soc.* **1998**, *120*, 3231−3236.

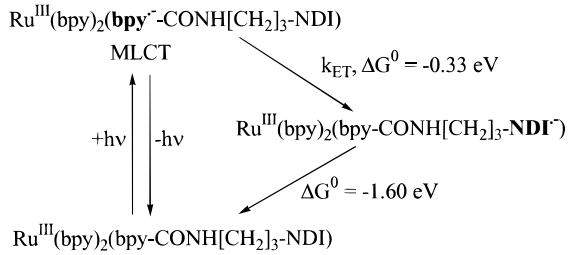

Figure 9. Electron transfer reactions and free energy relationships for Ru−NDI **1**.

CONHR ligand in these complexes (Figure 9). It is likely that subsequent electron transfer reactions take place from this state because intramolecular equilibration of the higher-energy charge transfer states located on the two bpy ligands with that located on the bpy-CONHR ligand should be rapid relative to processes such as electron transfer quenching.[85,90]

The steady state emission and emission decay studies of **1** in buffer solution indicate that quenching of the $Ru^{III}(bpy)_2(bpy^{\bullet-}$-CONH) MLCT state by NDI is highly efficient. The emission lifetimes for **1** show that 99% of the luminescence from **1** is quenched at an average rate of 1.6×10^9 s^{-1} in solution. We assign the emission quenching in **1** to oxidative electron transfer from $[Ru^{III}(bpy)_2(\mathbf{bpy}^{\bullet-}$-CONH$[CH_2]_3)-$NDI] to $[Ru^{III}(bpy)_2$-(bpy-CONH$[CH_2]_3)-\mathbf{NDI}^{\bullet-}$] as displayed in Figure 9. Photoinduced intramolecular electron transfer is highly favorable within this complex because NDI is easily reduced [$E_{1/2}$(NDI/$NDI^{\bullet-}$) = −0.33 V vs SCE in H_2O][89] and photoexcited Ru-$(bpy)_3^{2+}$ is easily oxidized [$E_{1/2}(Ru^{3+}/Ru^{2+}) = 1.27$ V vs SCE in H_2O;[107] $E(0,0) = 1.93$ eV for the Ru model **2**]. The driving force was calculated from eq 2,

$$\Delta G^\circ = e[E_{1/2}(D^{\bullet+}/D) - E_{1/2}(A/A^{\bullet-})] - \Delta E(0,0) + w(r) \quad (2)$$

where e is the charge on the electron, $E_{1/2}$ is a half-wave reduction potential for either the donor ($D^{\bullet+}$/D) or acceptor (A/$A^{\bullet-}$) couples in volts, $\Delta E(0,0)$ is the energy of the Ru chromophore's MLCT state, and $w(r)$ is a Coulombic interaction term between the oxidized donor and reduced acceptor which represents energy stored in the ionic products due to separating them a distance r relative to each other;[108] $w(\infty) = 0$.[109,110] The Coulombic term is generally less than ca. 0.1 eV in polar solvents and is neglected here. On the basis of these values, the driving force ($-\Delta G^\circ$) for intramolecular forward electron transfer within this complex is approximately 0.33 eV.

Energy transfer from the Ru-centered MLCT state of **1** at 1.93 eV to the singlet excited state of NDI at 3.2 eV is too uphill to be responsible for the rapid MLCT state quenching observed in **1**. Triplet−triplet energy transfer from the Ru-centered MLCT state to the n,π^* triplet state of alkylated NDI at 2.05 eV[62,72] is uphill by ca. 0.12 eV. This reaction is spin-allowed by the exchange mechanism. However, when the triplet energy of the acceptor is equal to or greater than the triplet energy of the donor, triplet−triplet energy transfer rates are generally $\leq 10^6$ s^{-1}.[111] The observed $\langle k_{ET} \rangle$ of 1.6×10^9 s^{-1} for **1** is thus best assigned to an intramolecular electron transfer process given the estimated driving force of 0.33 eV for this reaction.

Assignment of the observed quenching as an electron transfer reaction is supported by a recent study of photoinduced intramolecular electron transfer in a closely related $Ru^{II}-[CH_2]_3-$NDI$-[CH_2]_3-Ru^{II}$ homodinuclear complex in acetonitrile solution by Haga and co-workers.[66] In this complex, the ruthenium centers were each chelated by two bipyridines and a symmetrical bis(2-pyridylbenzimidazolyl)$-[CH_2]_3-$NDI ligand. The Ru-centered MLCT state was located at 2.05 eV, and the driving force for formation of the $Ru^{III}-NDI^{\bullet-}$ state was 0.35 eV. At 200 ps after flash excitation with 532 nm light, absorption peaks characteristic of $NDI^{\bullet-}$ were observed in 80−100% yield ($k_{ET} \approx 90$ ps). The $Ru^{III}-NDI^{\bullet-}$ charge transfer product then decayed in 345 ps. The similar structures and driving forces for electron transfer for **1** and Haga's derivative, and the high yield of the naphthalene diimide radical ion in the latter, argue that quenching of the MLCT state in Ru−NDI **1** also occurs via electron transfer.

The multiexponential emission decay for **1** in buffer suggests that the relative separation and orientation of the donor and acceptor groups affect the electron transfer quenching rate within this complex. Although the emission decay for **1** in buffer is dominated (∼88%) by a subnanosecond-lived (340 ps) emissive species, there are also contributions from nanosecond-lived emissive species (2 ns, 11%, and 12.6 ns, 0.8%). These lifetimes likely represent average quenching rates within conformational families of the donor−acceptor complex where fractional amplitudes indicate relative populations of different conformer sets. Different conformations for **1** are expected because the flexible $-(CH_2)_3-$NHCO− linker connecting the Ru^{II} tris-bpy and NDI moieties in **1** allows a variety of geometries. It might be expected that interaction between the hydrophobic NDI and the bpy ligands on the metal center would be energetically favorable in a polar aqueous environment. Indeed, the NMR observations are consistent with a geometry in which the Ru-$(bpy)_3^{2+}$ moiety lies at least in part in the shielding cone above the naphthalene diimide ring.[83] Thus it is likely that in buffer the predominant conformations for **1** involve relatively close contact between the Ru and NDI centers. The 12 ns lived species could then represent less populated conformations where the donor and acceptor are spaced farther apart or where the orientation between donor and acceptor is less favorable for electron transfer.

Binding of Ru−NDI 1 to DNA. Naphthalene diimides with pendant side chains of various sizes are known to intercalate in double-stranded DNA.[73,74,76] Both the UV−visible absorbance and induced CD spectra of **1** in the presence of DNA provide evidence that **1** binds to DNA by way of intercalation. This evidence includes (1) a significant degree of hypochromism (48−52%) in the absorbance for the NDI moiety in **1**, close to the extent of the hypochromism observed for a model NDI under the same conditions; and (2) a strong negative induced CD band in the region of the NDI absorbance bands nearly identical to the induced CD spectrum of the model NDI. Taken together, these optical signatures of **1** bound to DNA strongly suggest that the NDI chromophore in **1** intercalates between base pairs in the DNA. The fact that the absorbance changes for **1** in DNA are nearly identical to those for the model **3** in DNA suggests that the large Ru chromophore on one side chain of **1** does not significantly inhibit its binding to DNA. The observation that the MLCT absorbance band associated with the Ru chromophore of **1** does not show an induced circular dichroism spectrum when

(107) Scott, J. R.; Willie, A.; McLean, M.; Stayton, P. S.; Sligar, S. G.; Durham, B.; Millett, F. *J. Am. Chem. Soc*. **1993**, *115*, 6820−6824.
(108) Rehm, D.; Weller, A. *Isr. J. Chem*. **1970**, *8*, 259−271.
(109) Brunschwig, B. S.; Ehrenson, S.; Sutin, N. *J. Phys. Chem*. **1986**, *90*, 3657−3665.
(110) Sutin, N.; Brunschwig, B. S.; Creutz, C.; Winkler, J. R. *Pure Appl. Chem*. **1988**, *60*, 1817−1830.
(111) Turro, N. J. *Modern Molecular Photochemistry*; Benjamin/Cummings: Menlo Park, CA, 1978; pp 332−334.

bound to DNA indicates that it interacts only weakly with the DNA duplex. This is in line with previous studies which have shown that $Ru(bpy)_3^{2+}$ itself binds only weakly to the DNA, with a binding constant of only approximately 7×10^2 M^{-1} (50 mM phosphate, pH 7).[86,95] In addition, $Ru(bpy)_3^{2+}$ shows no change in the absorption maximum and no hypochromism upon the addition of DNA ([DNA]/[Ru] = 40, 5 mM Tris, 50 mM NaCl).[112] The low affinity of DNA for $Ru(bpy)_3^{2+}$ presumably arises because the cation interacts almost exclusively via electrostatic attraction to the negatively charged phosphates along the outside of the helix.[113]

Photophysical Studies of Ru−NDI 1 in DNA. The photophysical behavior of **1** when bound to DNA shows only small changes in comparison to its photophysical characteristics in solution. The most prominent change in the emission decay of **1** upon binding to DNA is the 10-fold increase in fractional amplitude of the longest-lived emission (to 0.08, 11.8 ns) concomitant with a 10% decrease in the fractional amplitude of the shortest-lived emission (to 0.79, 0.31 ns) relative to the decay of **1** in solution without DNA (Table 1). These changes result in an overall *reduction* of a factor of 2.4 for the average electron transfer rate of **1** intercalated in DNA compared to its rate in solution without DNA. It is striking that while the distribution of fractional amplitudes for the emission lifetimes of **1** changes upon DNA binding, the lifetimes themselves remain essentially the same. Also, the shortest emission quenching times are nearly the same in DNA or in buffer lacking DNA. Indeed most (79%) of the electron transfer quenching of the ruthenium moiety's MLCT state still occurs in ca. 300 ps for **1** in DNA as it does in aqueous solution (88%). This suggests either that the DNA environment experienced by the intercalated NDI moiety does not significantly alter the electronic coupling and activation energy for intramolecular electron transfer in this complex or that such changes cancel fortuitously.

Acknowledgment. This work was supported in part by the National Institutes of Health (AI127196 to D.W.D.) and the National Science Foundation (CHE-9709318 to T.N.).

IC971446S

(112) Yang, G.; Wu, J. Z.; Wang, L.; Ji, L. N.; Tian, X. *J. Inorg. Biochem.* **1997**, *66*, 141−144.
(113) Kalsbeck, W. A.; Thorp, H. H. *J. Am. Chem. Soc.* **1993**, *115*, 7146−7151.